The DREAM: An Integrated Photonic Thresholder

Alexander N. Tait, *Student Member, IEEE*, Bhavin J. Shastri, *Member, IEEE*, Mable P. Fok, *Member, IEEE*, Mitchell A. Nahmias, *Student Member, IEEE*, and Paul R. Prucnal, *Fellow, IEEE*

Abstract—We propose a novel all-optical integrated thresholder called the dual resonator enhanced asymmetric Mach–Zehnder interferometer (DREAM). Unlike prior integrated photonic devices, the DREAM exhibits properties of stable binary decision making, outputting a constant "one" power value for signals above a certain power level and "zero" for signals of lower powers. This thresholding shape arises from the interference of complementary nonlinear effects of two microring resonators (MRR), one in each arm of a Mach–Zehnder interferometer (MZI). The proposed device performs several orders of magnitude better in size, decision latency, energy efficiency, and stability compared to fiber-based methods of optical thresholding. It is best suited for application in densely integrated systems where rapid conversion between analog and digital signal domains is ubiquitous, such as hybrid analog-digital and neuromorphic processing architectures.

We derive analytical steady-state solutions to the nonlinear MRR, which enable design simulation, optimization, and automation of a continuous signal thresholder about three orders of magnitude faster than with numerical simulation. Additional numerical simulations indicate the possibility of a 50 GHz pulse thresholder with a 380 pJ switching threshold in a silicon-on-insulator (SOI) platform. The proposed circuit design techniques are potentially applicable to a wide range of materials, waveguide platforms, and resonator types, but for concreteness, we limit the focus of this paper to MRRs in SOI.

Index Terms—Integrated optics, interferometry, microresonators, silicon on insulator technology, threshold logic devices.

I. INTRODUCTION

THRESHOLDERS are the simplest kind of binary decision maker, outputting "one" if a signal is above a certain threshold value and "zero" if below. Much more than digital logic buffers, thresholders are analog-input, digital-output devices that allow a physical interface between these representational domains. They are found at the heart of digital-to-analog converters, comparators, and operational amplifiers [1]. Thresholding also plays a central role in processing architectures with ubiquitous conversion between analog and digital domains, such as spiking neural networks [2]. A spiking photonic neuron computational primitive was recently reported [3]–[5], but its scalability to larger systems hinges on improvements in thresholder performance. All-optical nonlinear processing devices have long been sought to reduce the strain on optical-electronic-optical conversion in high-capacity fiber communication systems. As optical interconnects find application at progressively shorter scales in computing systems, reliable, integrable, and efficient all-optical processing devices will become especially critical to support speed and energy performance scaling. Integrated devices that can reduce noise corruptions to a binary signal have been demonstrated [6]; in contrast, a thresholder must produce an approximately binary output from on a continuous valued analog input signal, thus making a decision. Ultrafast all-optical thresholders have previously been constructed using fiber based interferometers [7], [8]; however, the long interaction lengths required for switching in nonlinear fibers (meters to kilometers) and transfer function ripple in the above-threshold one-level region limit these techniques to specialized applications.

Microring resonators (MRR) exhibiting a Kerr nonlinearity can be used to considerably reduce the area and power needed to achieve self-switching by increasing the effective interaction length and instantaneous optical powers through coherent power buildup [9]. The thresholder described in this paper is five orders of magnitude smaller and exhibits four orders of magnitude shorter decision latencies and three orders of magnitude lower threshold powers than a fiber thresholder. Table I summarizes key performance criteria. Although resonant enhancement of nonlinearity reduces the available bandwidth, the small size of MRRs maintains the ability to respond on ultrafast timescales. The throughput of fiber thresholders can be very high, making them well-suited to communications; however, the latency of a given pulse is very long (ns) due to the slow nonlinear phase accumulation in a long fiber. In computing systems where logical feedback is employed, this decision latency is a much more important metric than throughput in determining system operation speed.

Thresholders are characterized in large part by their nonlinear transfer function of output energy against input energy, which is ideally the shape of a step function. Past experiments with a single resonator enhanced MZI (REMZ) have demonstrated that the shape of the energy transfer function is piecewise linear until a smooth saturation, unlike the piecewise constant step function required for thresholding [10]–[12]. This behavior, often called self-switching, is common in many nonlinear optical devices [13]–[17]; however, none to the authors' knowledge are suitable for thresholding due to the lack of a flat one-level region. We would like to emphasize the difference between a non-

A. N. Tait, B. J. Shastri, M. A. Nahmias, and P. R. Prucnal are with the Lightwave Communications Laboratory, Department of Electrical Engineering, Princeton University, Princeton, NJ 08544 USA (e-mail: atait@princeton.edu; shastri@ieee.org; mnahmias@princeton.edu; prucnal@princeton.edu).

M. P. Fok is with the Lightwave and Microwave Photonics Laboratory, College of Engineering, University of Georgia, Athens, GA 30606 USA (e-mail: mfok@uga.edu).

TABLE I
COMPARISON OF THRESHOLDING PERFORMANCE CRITERIA FOR THREE
DEVICES. PARAMETERS FOR THE REMZ AND DREAM CORRESPOND TO 4 μm
RADIUS MICRORINGS IN SOI

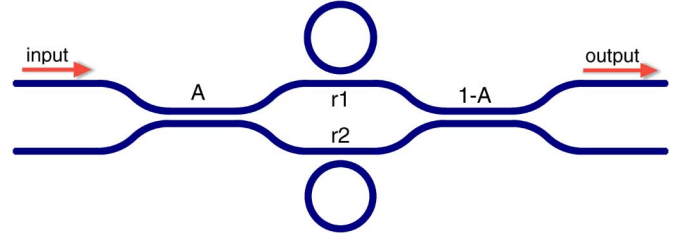|	NOLM [7]	REMZ	DREAM
Size	4 cm^2	6×10^{-5} cm^2	7.5×10^{-5} cm^2
Latency	4.5×10^4 ps	10 ps	10 ps
Throughput	400 GHz	100 GHz	100 GHz
Energy efficiency	1%	90%	40%
π-power	40dBm	-6dBm	-5dBm
One-level stability	ripple	increasing	flat

Fig. 1. The DREAM layout. While not visible in the layout diagram, asymmetry between the two arms is due to a coupling ratio A that is not -3 dB, a difference between MRR coupling parameters r_1 and r_2, and a fixed arm length difference.

linear transmission function, which has the ratio of output to input as the dependent variable, and a nonlinear transfer function, which instead plots the output as a function of the input (Fig. 2). Ideal self-switching devices exhibit step-like *transmission* functions; however, this corresponds to piecewise linear *transfer* functions unsuitable for thresholding. In [18], an interferometer with side-coupled and in-line MRRs was simulated, but only in steady-state and not in the context of signal processing. In our treatment, the transient response of a device to pulsed inputs are explored for more effective application to thresholding operation.

In this paper, we will greatly expand on the analysis and design methods pertaining to results originally presented in [19], in addition to showing new results of 50 GHz pulse thresholding. The dual resonator enhanced asymmetric MZI (DREAM), shown in Fig. 1, is similar to the REMZ, but eliminates its detrimental characteristics using the complementary action of two microresonators, one in each arm of a MZI. Since the transmission of an interferometer depends on the phase difference of two arms, undesirable elements of the natural MRR response can be made to interfere destructively, while a slight parameter asymmetry between the two MZI arms accentuates the net thresholding effect with flat levels representing zero and one. Because of its increased number of parameter degrees of freedom and a complex interplay of nonlinear elements, manual optimization of DREAM thresholding behavior can quickly overwhelm a designer. When using standard numerical finite difference time domain (FDTD) simulations, this optimization process also takes an impractically long time. To accelerate simulation, we have analytically derived approximate steady-state solutions of nonlinear MRR behavior and incorporated this solver into a fully automated DREAM optimization program. This new software design tool can automatically locate parameters that are optimal for thresholding by comparing hundreds of simulated transfer functions at a rate about three orders of magnitude faster than FDTD.

II. MODELING COMPLEMENTARY OPTICAL RESONATOR INTERFEROMETRY

In much the same way that a CMOS gate uses the complementary action of two similar, opposing components to achieve novel behavioral phenomena, the DREAM exhibits fundamentally new optical thresholding characteristics. To achieve a constant one-level value above threshold, the nonlinear transmission must decrease in inverse proportion to input power. Intuitively, this occurs if the bottom MRR has a smoother phase
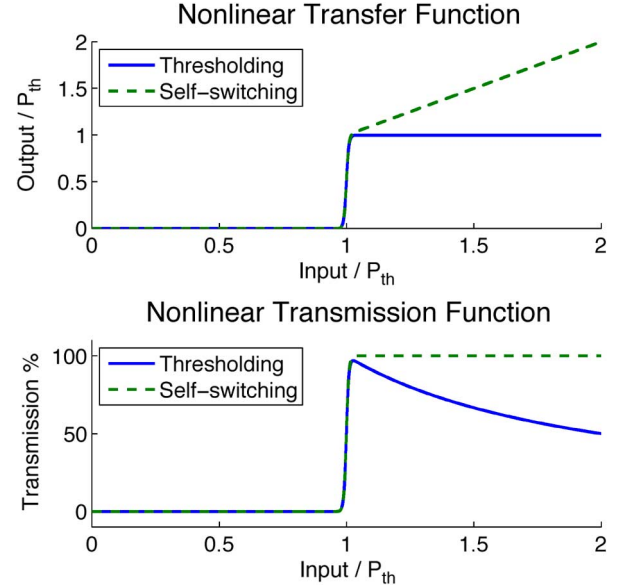

Fig. 2. A comparison of the nonlinear transfer function and the nonlinear transmission function for two ideal devices. The ideal thresholder has a transfer function that approaches a Heaviside step function, while the self-switching or transparency-inducing device has a step-like transmission function.

transfer characteristic that saturates at a higher input power/energy. The phase difference between the two arms will be similar below the sharp phase change in the upper arm, which leads to complete destructive interference. As the upper arm saturates in transmissivity, the lower arm phase transfer will begin to approach that of the upper arm above threshold, resulting in a net decreasing transmission function above threshold. With the available degrees of freedom, the opposing action of the MRRs can be tuned to provide the net desired thresholding shape. In terms of parameters, this means having a weakly coupled MRR (higher finesse) in the top arm and a moderately more strongly coupled MRR (lower finesse) in the bottom arm. The relative power saturation offset requires an asymmetric MZI coupler of power coupling ratio A less than 0.5 (-3 dB). To get complete destructive interference in the zero-level, the output coupler must then have the opposite power coupling ratio: $1 - A$.

In this section, we will add to the theory of nonlinear switching in microrings to obtain an analytical approximation to the phase transfer function of a MRR. For rapid optimization, we use a MATLAB script with an analytical approximation to the phase transfer function of a MRR to efficiently compute the power transfer function, which we score according to an

objective functional that favors functions of a step-like shape. A gradient descent algorithm minimizes this score. The roughly optimized parameters are then ported to a more physically accurate simulation in VPI Photonics software for verification.

A. An Analytic Steady-State Transfer Function

The nonlinear resonator is best understood in terms of the circulating power buildup factor $\mathcal{B}$ and single pass phase shift ϕ. The linear resonator equations dictate that the buildup factor is a peaked function of phase detuning from resonance. In the presence of nonlinearity, the phase also becomes dependent on the power circulating in the cavity, which is the product of incident power and its buildup factor. These two physical relationships between buildup and phase allow us to find a self-consistent operating point of the MRR in steady state. The resonance relationship of a linear MRR with round trip loss a and coupling parameter r can be expressed

$$\mathcal{B}(\phi) = \frac{a^2(1 - r^2)}{1 - 2ar\cos\phi + a^2 r^2}. \tag{1}$$

The phase difference acquired for a third order nonlinearity can be expressed as an intensity-dependent refractive index n_2. In a cavity, this phase shift from the small signal original ϕ_0 depends on $\mathcal{B}P$. This leads to the equation

$$\mathcal{B}(\phi) = \frac{\phi - \phi_0}{P} \frac{\lambda A}{2\pi L n_2} \tag{2}$$

where λ is the free space wavelength, and L is the effective round trip length of the microresonator ($2\pi R$ for a MRR of radius R).

By equating (1) and (2), we obtain a transcendental equation of ϕ; however, we would like to obtain analytical solutions for the sake of thresholder optimization acceleration, where hundreds or perhaps thousands of transfer functions are simulated and compared. To capture the switching properties of MRRs, we need only be concerned with $\mathcal{B}$ around one narrow resonance peak of phase width on the order of $2\mathcal{F}^{-1}$ for resonators with finesse greater than 5. In this domain of interest, a quadratic approximation for $\cos\phi$ has error bounded to less than 10^{-3}, so we will make a Lorentzian approximation to the resonance peak centered at ϕ_0 in (1):

$$\frac{\phi - \phi_0}{P_1} \frac{\lambda A}{2\pi L n_2} \approx \frac{a^2(1 - r^2)}{1 - 2ar\left(1 - \frac{1}{2}\phi^2\right) + a^2 r^2} \tag{3}$$

We then obtain a cubic equation, which has well known solutions.

$$\begin{aligned} [ar] \quad & \phi^3 \ldots \\ +[-ar\phi_0] \quad & \phi^2 \ldots \\ + \left[(1 - ar)^2\right] \quad & \phi \ldots \\ + \left[-(1 - ar)^2\phi_0 - \frac{2\pi L n_2}{\lambda A}a^2(1 - r^2)P_1\right] \quad & = 0 \end{aligned} \tag{4}$$

This equation can be solved analytically with the cubic formula to find the function $\phi(P)$. Cubics are guaranteed to have at least one real root, and some have three real roots. In the case

of the nonlinear resonator, values of P for which there are three real roots are regions of bistability; the medial root being an unstable solution. The one or two stable solutions for $\phi(P)$ given by the cubic formula are substituted into

$$t(\phi(P)) = \frac{E_2}{E_1} = e^{i(\pi + \phi)}\frac{a - re^{-i\phi}}{1 - are^{i\phi}} \tag{5}$$

to give the complex transmission of a nonlinear microring.

B. DREAM Analytics

The DREAM has five design degrees of freedom (A, r_1, r_2, ϕ_0, and Φ_b); where A is the power coupling ratio of the asymmetric MZI; $r_1(r_2)$ is the amplitude self-coupling coefficient (i.e., reflectance) of the directional coupler to the MRR in the top (bottom) arms, which is directly related to the finesse of each resonator; ϕ_0 is the initial offset in radians from the resonance condition, which is controlled by the optical wavelength of the input; Φ_b is the fixed phase bias between the two arms. The sensitivity of the response to the input wavelength (via ϕ_0) means the power transfer functions of a given design are only valid for a single operating wavelength.

The DREAM has one microring in each arm and an additional phase bias Φ_b that results from a path length difference between the two arms. It's output power is

$$\begin{aligned} P_{\text{out}} &= A(1 - A)P_{\text{in}}\left|t_1 - e^{i\Phi_b}t_2\right|^2 \\ \text{where } t_1 &= t(\phi_1(A \cdot P_{\text{in}})) \\ \text{and } t_2 &= t(\phi_2((1 - A) \cdot P_{\text{in}})) \end{aligned} \tag{6}$$

C. MZI Biasing

The fixed phase difference between the two arms of the MZI is set in order to get maximum destructive interference for small signal inputs that are below threshold. Its optimal value can be determined *a priori* to thresholding simulations; however, this optimum depends on the other degrees of freedom. The small signal (linear) phase shift imparted by a MRR of a certain coupling ratio and single-pass phase offset ϕ_0 is straightforward to derive [9]. The net phase difference can be cancelled by biasing Φ_b to satisfy the equation

$$\begin{aligned} \Phi_b = {}&\arctan\left(\frac{r_2\sin\phi_0}{a - r_2\cos\phi_0}\right) + \arctan\left(\frac{ar_2\sin\phi_0}{1 - ar_2\cos\phi_0}\right) \ldots \\ &- \left[\arctan\left(\frac{r_1\sin\phi_0}{a - r_1\cos\phi_0}\right) + \arctan\left(\frac{ar_1\sin\phi_0}{1 - ar_1\cos\phi_0}\right)\right]. \end{aligned} \tag{7}$$

III. THRESHOLDER OPTIMIZATION

A. Optimization Software Using Analytic Solutions

We have so far described how the transfer function can be derived analytically from device parameters, but there are several other modules required for automated optimization. Minimization algorithms require a scalar objective function that is defined on the parameter space. There are several distinct features of interest for thresholding, including flatness of the zero-level regime, flatness of the one-level regime, sharpness of the transition, width of the bistable region, absolute threshold power, and
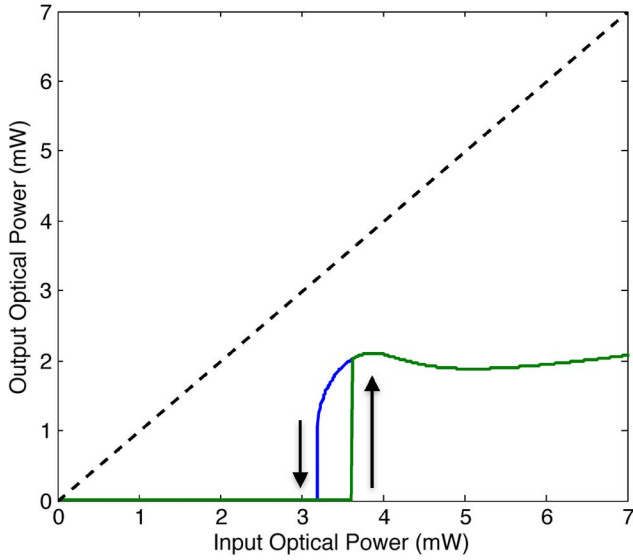
Fig. 3. Analytically optimized steady-state power transfer function simulated and optimized by the developed MATLAB program. The curve has a bistable region, where the response to increasing inputs is shown in green and decreasing inputs in blue (direction indicated by arrows). Device parameters are $\{A = 0.483, r_1 = 0.966, r_2 = 0.979, \phi_0 = -0.0481, \text{ and } \Phi_b = -0.667\}$.
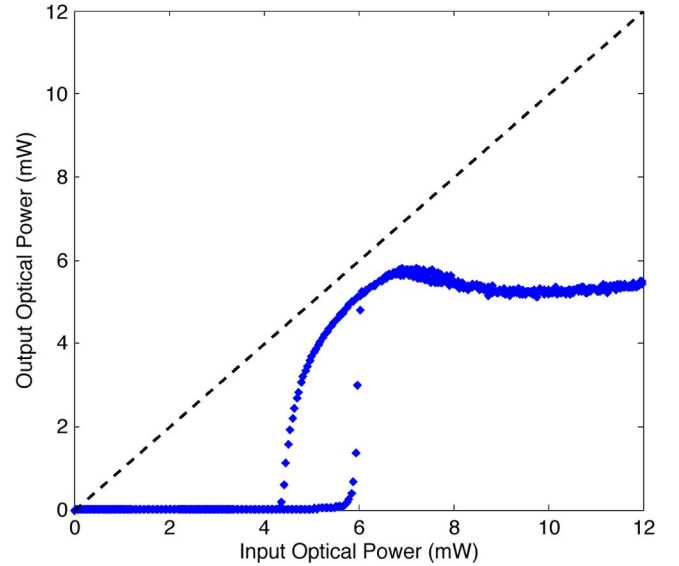

Fig. 4. Numerical FDTD simulation of a continuous signal thresholder simulated in VPI Photonics. Device parameters are identical to those used in Fig. 3. Input was a very slowly varying up- and down-ramp that allowed the device to settle very near its steady-state value. Bistability is visible.

power efficiency. All of these aspects can be quantified concretely.[1] We use a simple weighted sum of these aspects as a scalar objective function. Different applications may want to weight aspects differently or boost these aspects into a higher-dimensional parameter space for more advanced metric optimization. The objective function approach radically alters design flow by allowing top down thresholder design from the system level, rather than bottom up from the physical basis.

A MATLAB program was written to perform the above analytical simulation of the nonlinear transfer function and objective scoring function. The physical simulator and scoring function are referenced by a standard simplex minimization algorithm. An optimized transfer function discovered by this program is plotted in Fig. 3. Because each iteration of the optimizer is completely analytical, a local optimum can typically be determined in 3–5 seconds. The optimizer was clocked simulating 18 transfer functions per second, which represents a speedup over numerical FDTD by a factor of about 5,000.

Although analytical discussion thus far was platform independent, we simulate a device with material parameters corresponding to an SOI strip waveguide platform, for which refractive index $n = 3.45$, loss $\alpha = 2.4\,\mathrm{dB/cm}$ [20], intensity-dependent refractive index $n_2 = 7.5 \times 10^{-14}\,\mathrm{cm^2/W}$, and mode cross section $A_{\mathrm{eff}} = 1.2 \times 10^{-10}\,\mathrm{cm^2}$, The MRR radius is 4 μm and excitation wavelength very near 1.5 μm. All simulations in this paper will use these same platform values for the sake of specificity. A detailed characterization of parameter variation and its effects on transfer function shape was not developed during this study; however, based on simple manual variation of parameters, we estimate that the device precision required for exper-

imental observation of a thresholding curve is in the range of 1–5%. In some figures, three digit precision is used to specify device parameters for the sake of exactness and is not meant to represent digit significance.

B. Simulator Verification With VPI

Once optimized parameters were found in MATLAB, an analogous FDTD simulation was conducted in the more physically accurate VPI Photonics simulation environment in order to validate the essential predictions of the analytical model. Because of its numerical rigor, FDTD is a comparatively slow method that takes about 5 minutes to obtain a single transfer function. The simulated power transfer function for steady-state operation is shown in Fig. 4. Its shape is very similar to the analytically derived transfer function from Fig. 3. The absolute switching levels are lower in the analytical curve (3.2 mW versus 4.2 mW), a discrepancy that we postulate is due to small errors introduced by the approximations made during the analytical derivation. Although apparently not perfect for determining the exact threshold power, the analytical model of a MRR proposed in Section II is a valid model for transfer function shape optimization and parameter discovery: typically the most difficult aspects of DREAM design.

The effects of noise and signal transients on a continuous signal thresholder are shown in Fig. 5, for an example sinusoidal input at 0.5 GHz. Fig. 5(d) shows the output when the input is very noisy. Because of the flatness of both zero- and one-levels, the noise corruptions are reduced by the DREAM, yielding an output that is similar to the unperturbed example in Fig. 5(b). The DREAM reduces low amplitude noise that is in-band and/or broadband, unlike any linear element (e.g., a filter). The times of rising and falling edges still have high variance, but it is impossible for any asynchronous, causal system to remove this temporal uncertainty when given an uncertain input.

---

[1]Unlike with signals represented by electric voltage, optical signal values are directly linked to energy, so an ideal thresholder must throw out at least half of the input energy on average. We use a definition of power efficiency that is the ratio of one-level power to switching power, which can range from 0% to 100% (ideal).
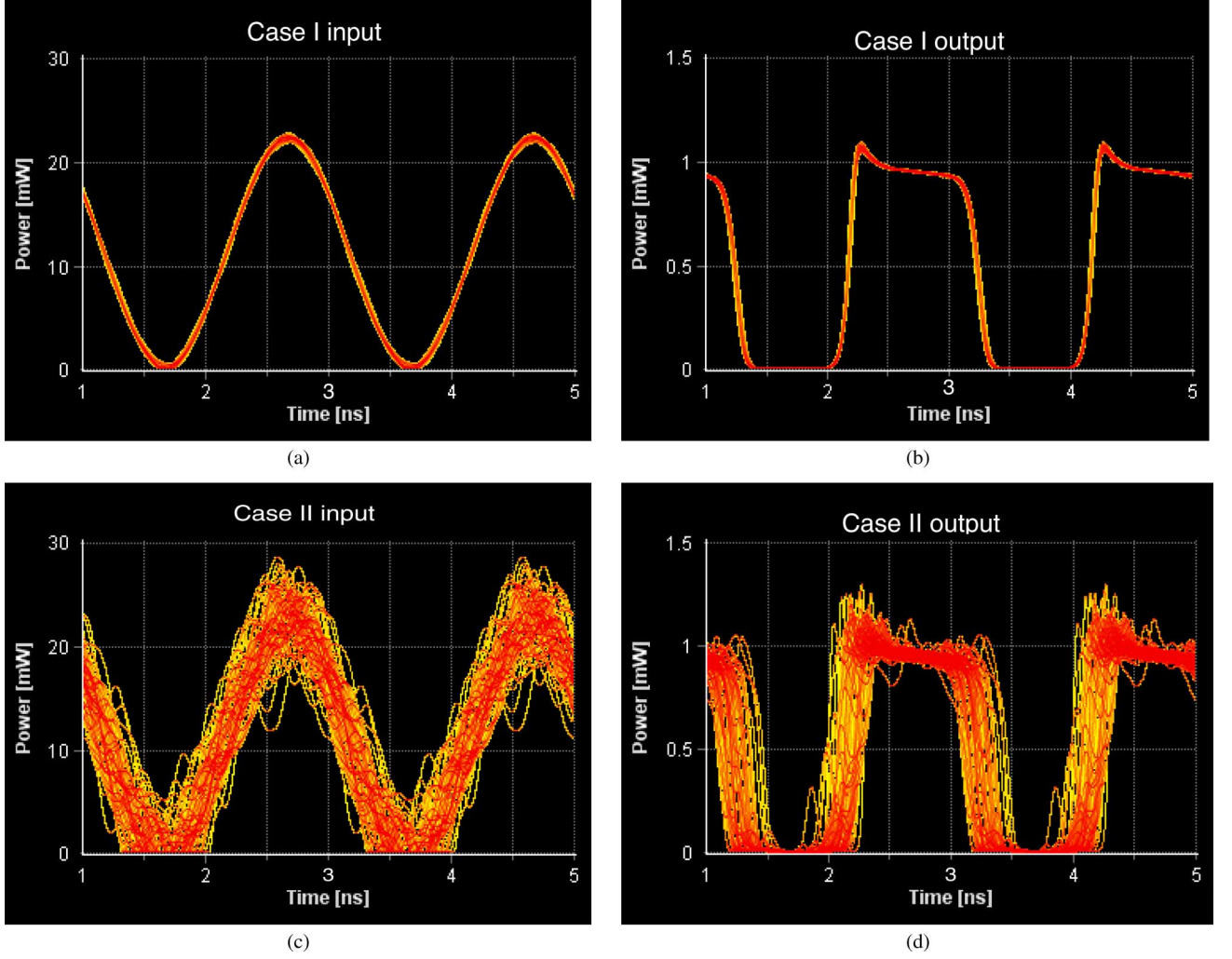
Fig. 5. Eye diagrams of time-domain simulations showing DREAM thresholding of continuous-time analog signals. Inputs are 0.5 GHz sinusoids with small (Case I) and large (Case II) noise corruption. (Color online). (a) Case I input; (b) Case I output; (c) Case II input; (d) Case II output.

Nonideal transient effects are best observed in Fig. 5(b). We observe a small transient overshoot at the rising edge, not encompassed by the steady-state model. The durations of rising and falling switching edges differ due to dynamical differences between positive feedback in coherent power buildup (rising edge) and power discharge by ring down (falling edge). Maximum operating speed is limited by the falling edge duration. In this case, we see that a falling edge duration of 250 ps when using 4 μm radii MRRs limits effective operation throughput to 2 GHz. Inputs with bandwidths higher than 2 GHz will not only experience significantly reduced sensitivity, but may create intermediate limit cycle responses that destroy the binary output behavior predicted by steady-state analysis. The relatively long discharge time of resonators limits the speed of the DREAM for continuous signal thresholding, but this limit is based on a near-steady-state analysis. We will find that this speed limitation does not apply in the case of pulsed inputs.

IV. PULSED MODE OPERATION

Thus far, we have analyzed models of the DREAM in the steady-state and simulations of continuous-time signal thresholding, which approaches steady-state behavior in the slowly varying limit. Many applications however require pulsed mode

operation, in which transient behavior will play a fundamentally significant role. Where intuition gained from steady-state analysis is valuable, we may refer below to pseudo-steady-states that are reached on sub-pulse timescales. Although we may also refer to bistable properties of these pseudo-steady-states, pulsed thresholders do not exhibit hysteresis. All circulating optical energy is allowed to discharge between input pulses, so the device begins in a common initial state for each pulse. Pulses are more appropriately described by their energy as opposed to peak or average power, so the power transfer function is here replaced by the energy transfer function. As with many dynamical systems, behavioral phenomena can be radically different in regimes where time scales of different processes are comparable or different. For photonic resonator switching, the relevant time scales are the cavity lifetime $[\tau_c = \mathcal{F} \cdot nL/(2\pi c)]$ and the input pulsewidth $[\tau_p]$. We will explore two limiting cases, designated "long" and "short" pulse thresholding, that correspond to $\tau_p > \tau_c$ and $\tau_p \approx \tau_c$, respectively. Pulsed thresholding results are obtained by standard FDTD simulation in VPI Photonics.

A. Long Pulse Thresholding

An energy transfer function for long pulse thresholding is shown in Fig. 6. Input pulses have widths of 113 ps, and MRRs
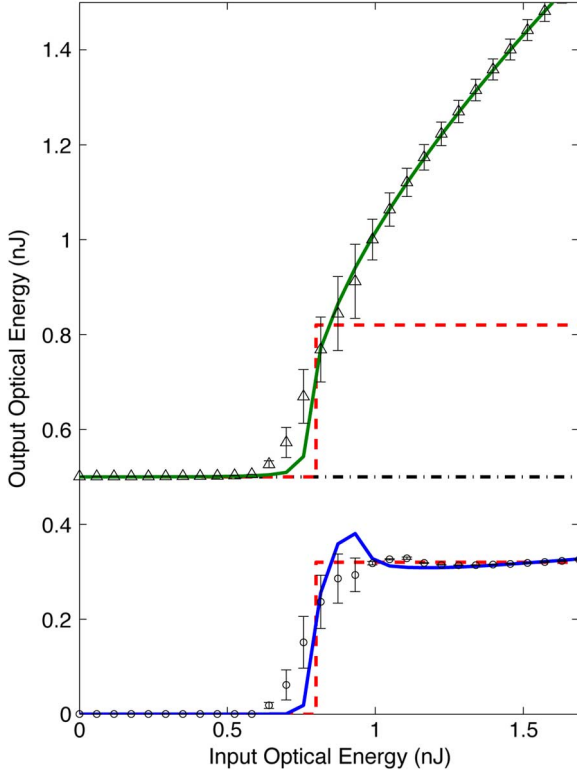
Fig. 6. Long pulse (113 ps) energy transfer functions of a DREAM (bottom, blue) and REMZ with identical device parameters (top, green, vertical offset 0.5 nJ). Solid lines correspond to noiseless inputs, while points and error bars indicate output mean and variance in the presence of -7.8 dBW noise power. Red dashed traces show ideal thresholding behavior. Device parameters are $\{A = 0.440, r_1 = 0.980, r_2 = 0.972, \phi_0 = -0.0559, \text{and } \Phi_b = -0.237\}$.
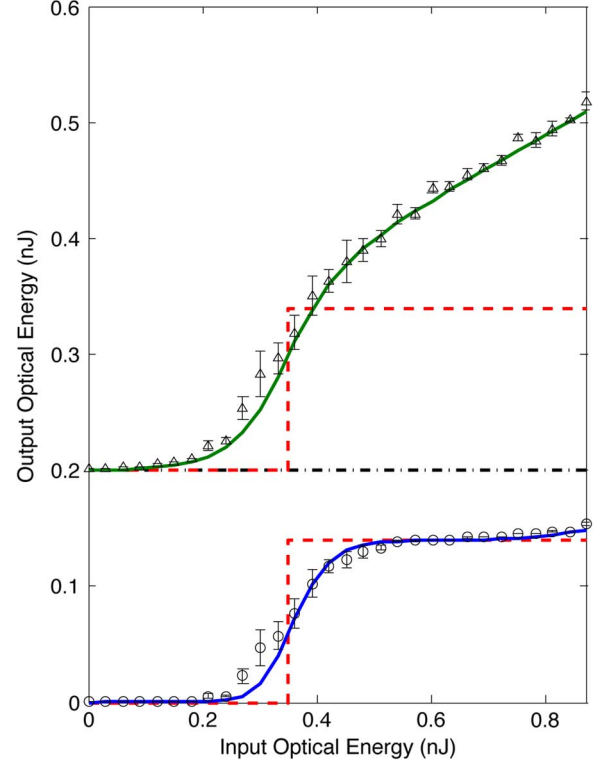

Fig. 7. Short pulse (16 ps) energy transfer functions of a DREAM (bottom, blue) and REMZ with identical device parameters (top, green, vertical offset 0.2 nJ). Solid lines are obtained for noiseless inputs. Points and error bars show mean and variance of output energies in the presence of 0.86 dBW noise power. Device parameters are $\{A = 0.46, r_1 = 0.980, r_2 = 0.964, \phi_0 = -0.0733, \text{and } \Phi_b = -0.376\}$.

have effective path lengths of 25 μm (4 μm radius). In contrast to a REMZ with identical device parameters (besides arm bias Φ_b), the DREAM achieves a step-like transfer function with flat zero- and one-level regions. Bandwidth is 8 GHz and switching energy is 800 pJ. The primary nonideality is a one-level overshoot just above threshold, where a pulse transient causes temporarily insufficient interference between the two arms.

The same figure shows the effect of noisy inputs, which not only introduce variance into the output energy, but can shift mean outputs away from the noiseless case. Even though the noise power of -7.8 dBW is high, noise outside of the pulse interferes deconstructively in the MZI. Noise on the pulse is small compared with the peak power of the input pulse, which is 12 dBW near threshold. When an input is close to threshold, even an ideal thresholder will greatly amplify input noise. The degree to which noise is suppressed away from threshold is, in fact, directly linked with noise amplification at threshold. The DREAM responds to noise in a similar way, with uncertainty appearing around threshold. Away from threshold, its behavior is very robust to additive optical noise on the pulse in addition to uncertainty in its total energy.

B. Short Pulse Thresholding

Fig. 7 shows energy transfer function results for short pulse thresholding. Input pulses now have widths of 16 ps, while the MRR size is unchanged. Simulation results indicate the possibility of all-optical pulsed thresholding at 50 GHz speeds with a switching energy of 380 pJ, and 40% efficiency using parameters available with current SOI technology. The transfer function closely resembles a sigmoidal curve, and is very well behaved in the one-level region. The threshold transition for short pulses is smoother than the long pulse case because the device does not have enough time to settle to bistable pseudo-steady-states (see Section V-A for more detailed analysis). The DREAM very effectively suppresses noise on the input pulse away from threshold, but as with the long pulse case, noise near threshold causes significant output variance. Just below threshold, the mean noisy output energy departs slightly from the noiseless value. The corresponding energy transfer function of a REMZ is also shown in order to illustrate that its one-level region is neither constant nor robust to noise.

These short pulse thresholding results could be observed over a range of timescales as long as τ_c and τ_p scale together (e.g., for pulses of width 100 ps or 5 ps with MRRs of radius 31 μm or 1.5 μm, respectively). Pulses that are much shorter do not have enough time to excite a given cavity. For most applications where speed and pulse shape control are priorities, short pulse thresholding would be a preferable operating regime. Long pulse thresholding would be more appropriate if an extremely sharp threshold were required and one-level overshoot were tolerable. In reality, a continuum of behaviors between "short" and "long" pulse thresholding is possible. This regime could provide a good balance of different performance aspects for general applications; however, rigorous simulation studies
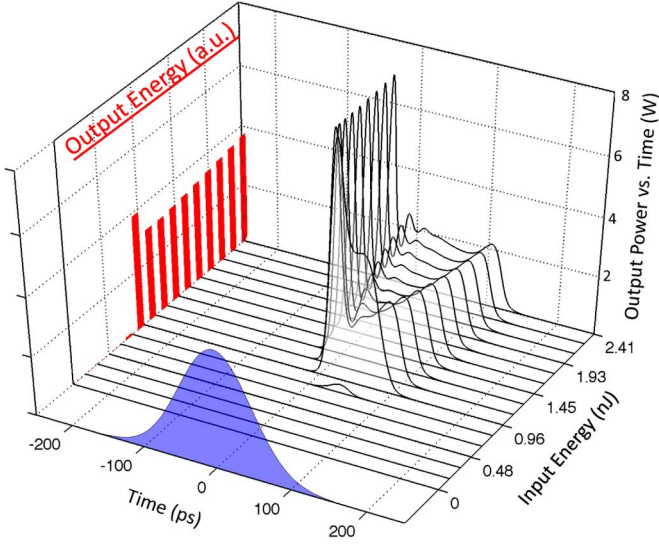
Fig. 8. 113 ps pulse shape distortion over the range of input energies. The input pulse shape is shown in blue on the same time axis, but with amplitude that depends on the trace. The time average of each trace (proportional to output energy) is displayed in red on the left y-z plane. At threshold, a high powered peak materializes, but does not increase above threshold. Output energy is held constant by a trailing plateau whose amplitude decreases as its width increases.
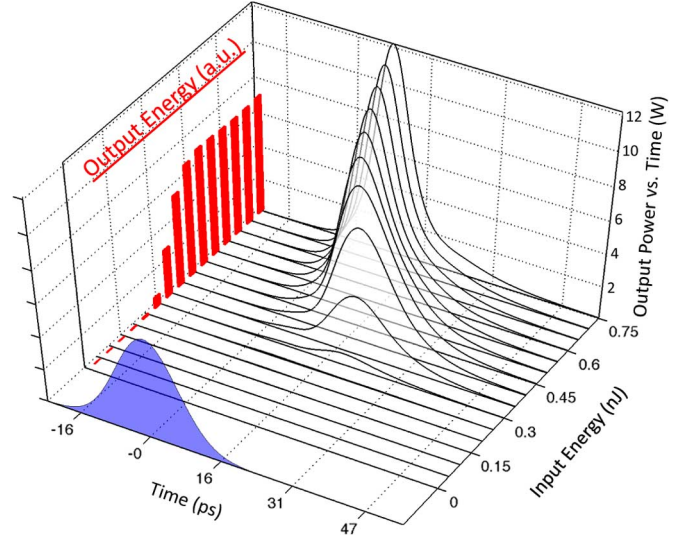

Fig. 9. 16 ps pulse shape distortion over the range of input energies. The input pulse shape is shown in blue on the same time axis, but with amplitude that depends on the trace. The time average of each trace (proportional to output energy) is displayed in red on the left y-z plane. As energy increases through threshold, the outgoing pulse center occurs earlier and has a higher peak intensity. At the same time, the outgoing pulses become narrower and acquire a tail.

of this wide regime will be impractical until more efficient numerical or semi-analytical methods of MRR simulation are conducted. Of course, a physical prototype would provide an ideal method for exploring this intermediate regime by using pulses of various widths.

V. DISCUSSION

A. Pulse Shape Distortion

The energy transfer function does not contain any information about the output pulse shape, which can be distorted. Pulse shapes for a range of input energies are shown in Fig. 8, corresponding to the long pulse (113 ps) regime. Although distortion is inconvenient in most photonic systems, it can typically be cleaned up by another device [6], [21]. The nature of the distortion can also help understand complicated internal resonator dynamics. Once enough power builds up in a resonator, the nonlinear phase-buildup feedback process takes over, causing a large jump in peak output power. The response overshoots, then rebounds to a minimum before eventually settling to a pseudo-steady-state. As input increases above threshold, the duration of this state increases, but its height decreases because of the opposing action of the other MRR. The net result is a distorted output pulse with constant energy. Due to the inherent nonlinearity of the system, the exact oscillation frequency of transients depends on input power, but can be seen to have an approximate timescale of 10 ps for the 4 μm MRRs.

One limitation of continuous signal thresholding is the long time it takes for circulating power built up in the resonators to ring down incoherently; however, by using pulses of duration on the order of transient oscillatory effects, we can realize a very fast coherent discharge. If we use short input pulses whose falling edges correspond with the rebound time of about 10 ps, the output pulse can rapidly return to zero. This optimization

technique is not exact, but after several iterations of observing pulse distortions at different input pulse widths, we have obtained and simulated an ultrafast 16 ps pulse thresholder. As seen in Fig. 9, 16 ps pulses do not give rise to pseudo-steady-state behavior, but instead cause a rapid return to zero power. The result is thresholding with 20 ps decision latency and very little pulse distortion.

Interpretations of pulse distortion will be an indispensable analytical tool for understanding the internal dynamics of an experimental device. In experimental studies, power and energy transfer functions could be readily observed, but internal nonlinear dynamics would be hidden. Pulse distortions would be one important observable that could augment the information used to guide tuning and optimization. An initial prototype would have to incorporate tunable couplers, which have been demonstrated for tuning the bandwidth of MRR filter response in SOI by [22]–[24].

B. Scaling Laws of Continuous and Pulsed Thresholding

The DREAM concept is independent of material, waveguide, and resonator types, making it applicable to several current photonic platforms and potentially even future platforms. The bandwidth and switching energy stand to improve as new materials that exhibit stronger nonlinear responses and new techniques for tighter mode confinement are developed. Overall performance can be quantified by the bandwidth-switching energy quotient [9],

$$\frac{B}{E_\pi} = \frac{1}{\sqrt{2\pi}} \frac{n_2 c^2}{L \lambda A_{\text{eff}} n^2 \ln 2} \propto L^{-1} \qquad (8)$$

where the switching energy E_π is defined as the energy required to cause a nonlinear phase change of π radians. A_{eff} is the waveguide effective cross-sectional area. This quotient is fixed for a

given material, wavelength, and waveguide geometry, but improved by shrinking microring path length. The balance between bandwidth and reduced switching energy is controlled through the finesse (determined by coupling ratio parameters). Since the pulse time is related to the round trip time and finesse of the cavity, the bandwidth-energy quotient can be converted to a bandwidth-power quotient that applies to continuous signal thresholding.

$$\frac{B}{P_\pi} = \frac{1}{\sqrt{2\ln 2}} \frac{\mathcal{F} n_2 c}{\pi \lambda A_{\text{eff}} n} \propto \mathcal{F} \qquad (9)$$

where P_π is the CW power required to elicit a π nonlinear phase shift. Unlike for pulsed operation, continuous signal thresholding performance increases with higher finesse, and the tradeoff between bandwidth and switching power is controlled by MRR length. This difference is highly relevant to the DREAM concept, in which we attempt to engineer the shape of a nonlinear transfer function using finesse as an important degree of freedom. That means the two goals of shape optimization and performance enhancement can conflict with one another. Although we have witnessed thresholding behavior over a range of finesse scales, the thresholding shape does in fact become difficult to control when finesse increases beyond about $\mathcal{F} \sim 200$ (i.e., $Q \sim 10^4$) (results not shown). Therefore, material technologies improving nonlinearity n_2 are required to scale continuous signal thresholding performance.

This design conflict is not shared by the case of pulsed mode thresholding. As long as the relation between L (or, more generally, resonator round trip time) and pulsewidth is maintained, the energy transfer function will maintain its shape, while performance improvement scales. This study has shown that a bandwidth-energy quotient of 1.3×10^{18} could be attained using 4 μm MRRs in SOI. MRRs with radii down to 1.5 μm have been demonstrated in this platform [25]. The apparent importance of resonant mode confinement might direct further investigations towards photonic crystal cavities, which have been shown to exhibit particularly tight confinement and high nonlinearity [14].

VI. Conclusion

We have proposed and simulated a novel integrated photonic thresholder based on complementary nonlinear resonator switching. The DREAM is the first integrated photonic device design to exhibit flat transfer regions above and below threshold, critical for thresholding analog input signals. Thresholding is unlike digital buffering because it makes a binary decision on a truly analog input. Several simulation studies indicate that the DREAM device can operate in several modes to threshold either continuous-time optical signals, "long" pulses slower than internal dynamics, or "short" pulses on the same time scale as internal dynamics. The proposed device is highly integrable (10^{-4} cm^2) with decision latencies about 3 orders of magnitude faster than state-of-the-art fiber thresholders. A naturally passive and energy efficient (40%) operation make the DREAM particularly well-suited for a silicon photonic platform. The technique of cavity enhancement of nonlinear effects carries with it a downside of strong wavelength sensitivity, which makes the transfer functions presented in this paper valid only for a given operating wavelength. The presence of

very different nonlinear responses to other wavelengths could potentially offer a means of all-optical threshold tunability.

Models of large-signal behaviors of nonlinear systems are typically limited to numerical methods such as FDTD that slow down design optimization and grant limited insight into the inner workings of such devices. By using a Lorentzian resonance approximation, we were able to develop an analytical steady-state model for the nonlinear MRR, which allowed rapid automation of a continuous-time signal thresholder. We have also conducted numerical simulation studies in VPI Photonics software to validate some analytical predictions about continuous signal thresholding. For pulsed mode thresholding, we have identified two qualitatively distinct short and long pulse regimes. Simulation results of short pulse thresholding indicate the possibility of 50 GHz, 380 pJ efficient thresholding with minimal pulse distortion using currently available SOI technology.

This paper has described the photonic analog of a circuit design technique, based very generally on Kerr nonlinearity, resonance, and interferometry. The DREAM concept could thus be applied to many different types of photonic platforms with a range of materials (i.e., SOI, III-V, chalcogenide), waveguide designs (i.e., slot [26], ridge, photonic crystal), and resonator geometries (i.e., microdisk, Bragg cavity, photonic crystal defect [14]). With advances in each of these technology centers, future thresholder performance could continue to improve, but the underlying concept of balancing undesirable responses of complementary resonators will remain relevant. Ongoing research will seek experimental demonstration of a DREAM thresholder and further explore the possibility of implementation in different kinds of optical resonators.

References

[1] G. C. Valley, "Photonic analog-to-digital converters," *Opt. Exp.* vol. 15, no. 5, pp. 1955–1982, Mar. 2007 [Online]. Available: http://www.opticsexpress.org/abstract.cfm?URI=oe-15-5-1955

[2] R. Sarpeshkar and M. O'Halleran, "Scalable hybrid computation with spikes," *Neural Comput.*, vol. 14, pp. 2003–2038, 2002.

[3] D. Rosenbluth, K. Kravtsov, M. P. Fok, and P. R. Prucnal, "A high performance photonic pulse processing device," *Opt. Exp.*, vol. 17, no. 25, pp. 22 767–22 772, 2009.

[4] M. P. Fok, H. Deming, M. Nahmias, N. Rafidi, D. Rosenbluth, A. Tait, Y. Tian, and P. R. Prucnal, "Signal feature recognition based on lightwave neuromorphic signal processing," *Opt. Lett.* vol. 36, no. 1, pp. 19–21, Jan. 2011 [Online]. Available: http://ol.osa.org/abstract.cfm?URI=ol-36-1-19

[5] M. P. Fok, Y. Tian, D. Rosenbluth, and P. R. Prucnal, "Asynchronous spiking photonic neuron for lightwave neuromorphic signal processing," *Opt. Lett.* vol. 37, no. 16, pp. 3309–3311, Aug. 2012 [Online]. Available: http://ol.osa.org/abstract.cfm?URI=ol-37-16-3309

[6] R. Salem, M. A. Foster, A. C. Turner, D. F. Geraghty, M. Lipson, and A. L. Gaeta, "All-optical regeneration on a silicon chip," *Opt. Exp.* vol. 15, no. 12, pp. 7802–7809, Jun. 2007 [Online]. Available: http://www.opticsexpress.org/abstract.cfm?URI=oe-15-12-7802

[7] K. Kravtsov, P. R. Prucnal, and M. M. Bubnov, "Simple nonlinear interferometer-based all-optical thresholder and its applications for optical CDMA," *Opt. Exp.*, vol. 15, no. 20, pp. 13 114–13 122, 2007.

[8] N. Rafidi, K. Kravtsov, Y. Tian, M. Fok, M. Nahmias, A. Tait, and P. Prucnal, "Power transfer function tailoring in a highly ge-doped nonlinear interferometer-based all-optical thresholder using offset-spectral filtering," *IEEE Photon. J.*, vol. 4, no. 2, pp. 528–534, Apr. 2012.

[9] J. Heebner, R. Grover, and T. A. Ibrahim, *Optical Microresonators: Theory, Fabrication, and Applications*, ser. Springer Series in Optical Sciences, W. Rhodes, Ed. New York, NY, USA: Springer-Verlag, 2008.

[10] J. Heebner and R. Boyd, "Enhanced all-optical switching by use of a nonlinear fiber ring resonator," *Opt. Lett.*, vol. 24, no. 12, pp. 847–849, 1999.

[11] T. Ibrahim, K. Ritter, V. Van, P. P. Absil, R. Grover, J. V. Hryniewicz, B. E. Little, F. G. Johnson, and P.-T. H.-T. Ho, "Experimental observations of optical bistability in semiconductor microring resonators," in *Integrated Photonics Research*, ser. OSA Trends in Optics and Photonics, A. Sawchuk, Ed. New York, NY, USA: Optical Society of America, 2001, vol. 58.

[12] V. Van, T. Ibrahim, P. Absil, F. Johnson, R. Grover, J. Goldhar, and P.-T. Ho, "All-optical nonlinear switching in gaas-algaas microring resonators," *IEEE Photon. Technol. Lett.*, vol. 14, no. 1, pp. 74–76, 2002.

[13] J. E. Heebner, P. Chak, S. Pereira, J. E. Sipe, and R. W. Boyd, "Distributed and localized feedback in microresonator sequences for linear and nonlinear optics," *J. Opt. Soc. Amer. B* vol. 21, no. 10, pp. 1818–1832, Oct. 2004 [Online]. Available: http://josab.osa.org/abstract.cfm?URI=josab-21-10-1818

[14] B. Maes, P. Bienstman, and R. Baets, "Switching in coupled nonlinear photonic-crystal resonators," *J. Opt. Soc. Amer. B* vol. 22, no. 8, pp. 1778–1784, Aug. 2005 [Online]. Available: http://josab.osa.org/abstract.cfm?URI=josab-22-8-1778

[15] S. Pereira, P. Chak, and J. E. Sipe, "Gap-soliton switching in short microresonator structures," *J. Opt. Soc. Amer. B* vol. 19, no. 9, pp. 2191–2202, Sep. 2002 [Online]. Available: http://josab.osa.org/abstract.cfm?URI=josab-19-9-2191

[16] S. Pereira, P. Chak, J. Sipe, L. Tkeshelashvili, and K. Busch, "All-optical diode in an asymmetrically apodized kerr nonlinear microresonator system," *Photon. Nanostructures—Fundamentals Appl.* vol. 2, no. 3, pp. 181–190, 2004 [Online]. Available: http://www.sciencedirect.com/science/article/pii/S1569441004000458

[17] Q. Xu and M. Lipson, "All-optical logic based on silicon micro-ring resonators," *Opt. Exp.* vol. 15, no. 3, pp. 924–929, Feb. 2007 [Online]. Available: http://www.opticsexpress.org/abstract.cfm?URI=oe-15-3-924

[18] Y. Lu, L. Xu, M. Shu, P. Wang, and J. Yao, "Proposal to produce coupled resonator-induced transparency and bistability using microresonator enhanced mach-zehnder interferometer," *IEEE Photon. Technol. Lett.*, vol. 20, no. 7, pp. 529–531, Apr. 2008.

[19] A. Tait, M. Nahmias, M. Fok, and P. Prucnal, "A dual resonator enhanced asymmetric Mach-Zehnder: Ultrafast passive thresholder for silicon-on-insulator," in *Proc. Int. Conf. OMN*, Aug. 2012, pp. 212–213.

[20] W. Bogaerts, R. Baets, P. Dumon, V. Wiaux, S. Beckx, D. Taillaert, B. Luyssaert, J. Van Campenhout, P. Bienstman, and D. Van Thourhout, "Nanophotonic waveguides in silicon-on-insulator fabricated with cmos technology," *J. Lightw. Technol.*, vol. 23, no. 1, pp. 401–412, 2005.

[21] J. E. Heebner, R. W. Boyd, and Q.-H. Park, "Scissor solitons and other novel propagation effects in microresonator-modified waveguides," *J. Opt. Soc. Amer. B* vol. 19, no. 4, pp. 722–731, Apr. 2002 [Online]. Available: http://josab.osa.org/abstract.cfm?URI=josab-19-4-722

[22] L. Zhou and A. W. Poon, "Electrically reconfigurable silicon microring resonator-based filter with waveguide-coupled feedback," *Opt. Exp.* vol. 15, no. 15, pp. 9194–9204, Jul. 2007 [Online]. Available: http://www.opticsexpress.org/abstract.cfm?URI=oe-15-15-9194

[23] L. Chen, N. Sherwood-Droz, and M. Lipson, "Compact bandwidth-tunable microring resonators," *Opt. Lett.* vol. 32, no. 22, pp. 3361–3363, Nov. 2007 [Online]. Available: http://ol.osa.org/abstract.cfm?URI=ol-32-22-3361

[24] Y. Ding, M. Pu, L. Liu, J. Xu, C. Peucheret, X. Zhang, D. Huang, and H. Ou, "Bandwidth and wavelength-tunable optical bandpass filter based on silicon microring-mzi structure," *Opt. Exp.* vol. 19, no. 7, pp. 6462–6470, Mar. 2011 [Online]. Available: http://www.opticsexpress.org/abstract.cfm?URI=oe-19-7-6462

[25] Q. Xu, D. Fattal, and R. G. Beausoleil, "Silicon microring resonators with 1.5-m radius," *Opt. Exp.*, vol. 16, no. 6, 2008.

[26] C. Koos, L. Jacome, C. Poulton, J. Leuthold, and W. Freude, "Nonlinear silicon-on-insulator waveguides for all-optical signal processing," *Opt. Exp.* vol. 15, no. 10, pp. 5976–5990, May 2007 [Online]. Available: http://www.opticsexpress.org/abstract.cfm?URI=oe-15-10-5976

Alexander N. Tait (S'11) received the B.Sci.Eng. (hons) in electrical engineering in 2012 from Princeton University, Princeton, NJ, USA, where he is currently working toward the Ph.D. degree in electrical engineering in the Lightwave Communications Group, Department of Electrical Engineering.

He was a research intern for the summers of 2008–2010 at the Laboratory for Laser Energetics, University of Rochester, Rochester, NY and an undergraduate researcher for the summers of 2011–2012 at the MIRTHE Center, Princeton University, Princeton, NJ. His research interests include photonic devices for nonlinear signal processing, integrated systems, neuromorphic engineering, and hybrid analog-digital signal processing and computing.

Mr. Tait is a Student Member of the IEEE Photonics Society and the Optical Society of America (OSA). He is a recipient of the National Science Foundation Graduate Research Fellowship. He is a co-recipient of the Optical Engineering Award of Excellence from the Department of Electrical Engineering at Princeton. He has co-authored 3 journal papers appearing in *Optics Letters*, the *Journal of Applied Physics*, and the *International Journal of Hydrogen Energy*.

Bhavin J. Shastri (S'03–M'11) received the B.Eng. (hons, with distinction), M.Eng., and Ph.D. degrees in electrical engineering from McGill University, Montreal, QC, Canada, in 2005, 2007, and 2011, respectively.

He is currently a Postdoctoral Research Fellow at the Lightwave Communications Laboratory, Princeton University, Princeton, NJ, USA. His research interests include ultrafast cognitive computing—neuromorphic engineering with photonic neurons, high-speed burst-mode clock and data recovery circuits, optoelectronic-VLSI systems, optical access networks, machine learning, and computer vision.

Dr. Shastri has garnered the following research awards: 2012 D. W. Ambridge Prize for the top graduating Ph.D. student, nomination for the 2012 Canadian Governor General Gold Medal, IEEE Photonics Society 2011 Graduate Student Fellowship, 2011 Postdoctoral Fellowship from National Sciences and Engineering Research Council of Canada (NSERC), 2011 SPIE Scholarship in Optics and Photonics, a Lorne Trottier Engineering Graduate Fellow, and a 2008 Alexander Graham Bell Canada Graduate Scholarship from NSERC. He was the recipient of the Best Student Paper Awards at the 2010 IEEE Midwest Symposium on Circuits and Systems (MWSCAS), the co-recipient of the Silver Leaf Certificate at the 2008 IEEE Microsystems and Nanoelectronics Conference (MNRC), the 2004 IEEE Computer Society Lance Stafford Larson Outstanding Student Award, and the 2003 IEEE Canada Life Member Award. Dr. Shastri was the President/Co-Founder of the McGill OSA Student Chapter.

Mable P. Fok (S'02–M'08) received the B.Eng., M.Phil., and Ph.D. degrees in electronic engineering from the Chinese University of Hong Kong (CUHK), Hong Kong, in 2002, 2004, and 2007, respectively.

She was a Visiting Researcher at the University of California, Los Angeles (UCLA), CA, USA, and the University of California, Santa Barbara (UCSB), CA, USA, during 2005 and 2006, respectively, where she was engaged in research on supercontinuum generation in nonlinear fibers with the former and all-optical processing of advanced modulation format signals with the later. After graduation, Dr. Fok joined the Department of Electrical Engineering at Princeton University, Princeton, NJ, USA, as an Associate Research Scholar in 2007, where she was focusing on hybrid analog/digital processing of optical signals based on neuromorphic algorithm and developing new techniques to enhance physical layer information security in optical communications network. She is currently an Assistant Professor with the Lightwave and Microwave Photonics Laboratory, University of Georgia College of Engineering, Athens, GA, USA. She has published over 120 journal and conference papers. Her recent research interest is on lightwave neuromorphic signal processing and developing new techniques to enhance RF wireless communications.

Dr. Fok is the recipient of the Special Merit in 2008 Hong Kong Institution of Science Young Scientist Awards, First Prize in 2007 IEEE Hong Kong Section Postgraduate Student Paper Contest, the 2006 Optical Society of America Incubic/Milton Chang Student Travel Grant Award, the 2005 IEEE Lasers and Electro-Optics Society Graduate Student Fellowship Award, and the 2005 Thomas HC Cheung Postgraduate Scholarship in Science and Engineering from the Hong Kong Association of University Women.

Mitchell A. Nahmias (S'11) received the B.S. degree (hons) in electrical engineering and a certificate in engineering physics from Princeton University, Princeton, NJ, USA, where he is currently pursuing the Ph.D. degree in electrical engineering under Prof. Paul Prucnal, continuing his undergraduate work on his excitable, photonic neuron.

Mr. Nahmias was a recipient of the John Ogden Bigelow Jr. Prize in Electrical Engineering and co-winner of the 'Best Engineering Physics Independent Work Award' for his senior thesis. He is a recipient of the National Science Foundation Graduate Research Fellowship.

Paul R. Prucnal (S'75–M'79–SM'90–F'92) received the A.B. degree (highest hons) from Bowdoin College (*summa cum laude*) in math and physics. He received the M.S., M.Phil., and Ph.D. degrees from Columbia University, New York, NY, USA.

He is currently a Professor of Electrical Engineering at Princeton University, where he has also served as the Founding Director of the Center for Photonics and Optoelectronic Materials, and is currently the Director of the Center for Network Science and Applications. He has held visiting faculty positions at the University of Tokyo and University of Parma.

Prof. Prucnal was an Area Editor of the IEEE TRANSACTIONS ON COMMUNICATIONS for optical networks, and was Technical Chair and General Chair of the IEEE Topical Meeting on Photonics in Switching in 1997 and 1999, respectively. He is a Fellow of IEEE with reference to his work on optical networks and photonic switching, a Fellow of the OSA, and a recipient of the Rudolf Kingslake Medal from the SPIE, cited for his seminal paper on photonic switching. In 2006, he was awarded the Gold Medal from the Faculty of Physics, Mathematics and Optics from Comenius University in Slovakia, for his contributions to research in photonics. He has received Princeton Engineering Council Awards for Excellence in Teaching, the University Graduate Mentoring Award, and the Walter Curtis Johnson Prize for Teaching Excellence in Electrical Engineering, as well as the Distinguished Teacher Award from Princeton's School of Engineering and Applied Science. He is editor of the book, *Optical Code Division Multiple Access: Fundamentals and Applications* (CRC, 2005).